Modelling of enhanced water flow in deformable carbon nanotubes using a linear pressure-diameter relationship

Ashish Garg[1,2,3*]

[1]Seminare Private Limited, Delhi, India

[2]Department of Chemical Engineering, Indian Institute of Technology Delhi, India

[3]Department of Mechanical & Aerospace Engineering, NIMS University, Jaipur, India

November 06, 2023

Abstract

Numerous researchers have documented a notable enhancement in water flow through nanotubes While modelling, these researchers typically treated the CNTs with rigid walls. The flow rates of water within carbon nanotubes (CNTs) are significantly influenced by the nanoconfined density, viscosity and the slip length. Despite considering substantial slip effects, there are unresolved findings of massive enhancements in flow rates. Recently, using a linear pressure-area relationship for the deformable tube walls, Garg [1] derived a model for the flow rates. In contrast to that, this paper takes a different approach, utilizing a small displacement structural mechanics framework with a linear pressure-diameter relationship, to incorporate the deformable nature of carbon nanotubes and derive another deformable model. We compare predicted flow rates with previous findings. The rigid-wall model with slips accurately predicted the outcomes of numerous studies. Nonetheless, we observed that in many studies featuring high porosity and thin-walled tubes, the inclusion of tube elasticity or deformability is crucial for accurate modeling. In such cases, our deformable-wall model with slips performed exceptionally well in predictions. We also compare and contrast the flow physics and flow rate scaling of the current model with the predictions from the Garg [1] deformable model. We also find that as the deformability $1/\beta$ increases, the flow rate also increases. Although the scaling for how the flow rate and flow physics varies are different than reported by Garg [1] with pressure-area model. We find that the flow rate in deformable tubes scales as $\dot{m}_{\text{deformable}} \sim 1/\beta^0$ for $\left(\Delta p/\beta\sqrt{A_o}\right) \ll 1$, $\dot{m}_{\text{deformable}} \sim 1/\beta$ for $\left(\Delta p/\beta\sqrt{A_o}\right) \sim O(10^{-1})$ and $\dot{m}_{\text{deformable}} \sim 1/\beta^4$ for $\left(\Delta p/\beta\sqrt{A_o}\right) \sim O(1)$. Further, for a given deformability factor β, the flow rate in the smaller diameter of the tube is much larger than the larger diameter where the flow rate increases with D_o^{-1} followed by D_o^{-4} as diameter decreases. We also find that for the rigid tube, the mass flow rate varies linearly with pressure, whereas for the deformable tubes, the flow rate scales as $\dot{m}_{\text{deformable}} \sim \Delta p^2$ for $\left(\Delta p/\beta\sqrt{A_o}\right) \sim O(10^{-1})$ during transition from $\dot{m}_{\text{rigid}} \sim \Delta p$ to $\sim \Delta p^5$, and finally to $\dot{m}_{\text{deformable}} \sim \Delta p^5$ for $\left(\Delta p/\beta\sqrt{A_o}\right) \sim O(1)$. On the otherhand, the scaling reported by Garg [1] was $\dot{m}_{\text{deformable}} \sim \Delta p^3$ for $\left(\Delta p/\alpha A_o\right) \sim O(1)$.

*Email: **ashish.garg.iisc@gmail.com, ashish@seminare.in**

https://doi.org/10.26434/chemrxiv-2023-k7mws **ORCID:** https://orcid.org/0000-0003-4544-7036 Content not peer-reviewed by ChemRxiv. **License:** CC BY-NC-ND 4.0

Keywords: deformable nanotubes, CNT, lubrication approximation, linear pressure-diameter relation, nanoconfined water

1 Introduction

The investigation into the transport behavior of water within nanopores holds great importance both in terms of fundamental understanding and practical applications. This significance arises from the widespread occurrence of nanopores in nature and their numerous technological uses [2–14]. Numerous researchers have documented a notable enhancement in water flow through nanotubes [9, 10, 15–17]. While modelling, these researchers typically treated the CNTs with rigid walls. The flow rates of water within carbon nanotubes (CNTs) are significantly influenced by the nanoconfined density, viscosity and the slip length. Despite considering substantial slip effects, there are unresolved findings of massive enhancements in flow rates [15, 17–23].

Recently, using a linear pressure-area relationship for the flexible tube walls, Garg [1] derived a model for the flow rates. In contrast to that, this paper takes a different approach, utilizing a small displacement structural mechanics framework with a linear pressure-diameter relationship [24], to incorporate the deformable nature of graphene-based nanotubes [25, 26]. Using similar methodology, as used by Garg [1], In this paper, we derive another deformable model incorporating linear pressure-diameter relationship and compare predicted flow rates with previous findings [9, 10, 15–23]. We also compare and contrast the flow physics and flow rate scaling of the current model with the predictions from the Garg [1] deformable model.

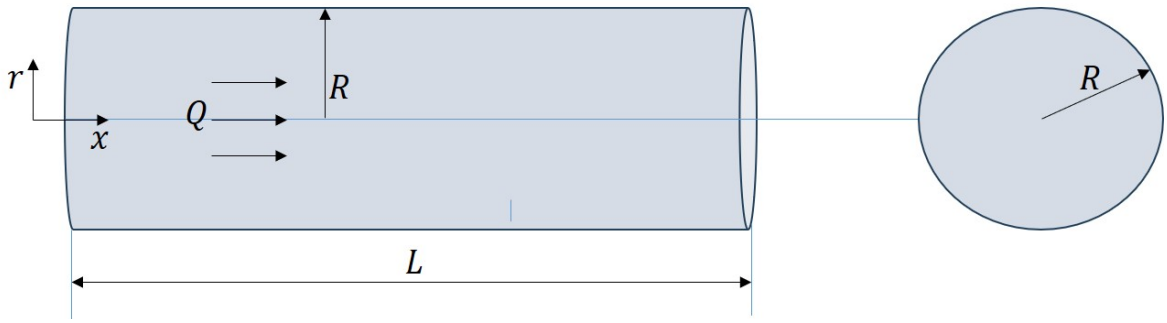

Figure 1: Schematic diagram of the flow Q in a graphene deformable-wall nanotube with length L and the cross-section radius R (diameter D).

We consider a slender nanotube with a length L and radius R (or diameter D), with $D \ll L$ as depicted in Figure 1 [27–30]. The tube's wall is flexible and deformable. The flow Q is induced by an applied pressure field along the x-direction. This flow exerts normal stresses on the tube's walls, causing radial deformation of the soft wall. At the reservoir (located at $x = 0$), a pressure field p is applied, while the exit pressure is set as a reference with a value of zero. At this point, we do not make specific assumptions about the magnitude of the deformable displacement, but we assume that the magnitude $|\delta| \ll D$ in our problem. Here, δ represents the change in radius due to wall deformation, expressed as $R = R_o + \delta$, where R_o signifies the initial or rigid wall tube radius, and R is the radius after tube wall deformation. The structure of this paper is organized as follows: Section 2 presents the model's derivation. In the Section 3, we present and analyze

https://doi.org/10.26434/chemrxiv-2023-k7mws **ORCID:** https://orcid.org/0000-0003-4544-7036 Content not peer-reviewed by ChemRxiv. **License:** CC BY-NC-ND 4.0

the results. Finally, we present conclusions in Section 4.

2 The Axisymmetric model: Involving microstructure of confined water

2.1 Structural small displacement mechanics: A linear pressure-area relationship

We use the relationship between local pressure and local diameter in deformable tubes, which is defined as the second model by Sochi [24], where the β defined in equation (1) is β'/A_o of the model. The model is

$$p = \beta(\sqrt{A} - \sqrt{A_o}), \tag{1}$$

where a linear correlation between pressure p and the change in radius or diameter $\sqrt{A} - \sqrt{A_o}$. Here, β represents the proportionality factor, which indicates the stiffness of the tube wall. A is the tube's cross-sectional area at the actual pressure p, and A_o is the initial tube area (or rigid tube-wall area) at the reference pressure (assumed to be zero for convenience). The model essentially states that the change in pressure at a specific point within the tube is directly proportional to the change in radius (or diameter) relative to its reference state. Please note that this model is different than what we used in our previous studies Garg [1], where we used linear Pressure-Area relationship instead of linear Pressure-Diameter.

2.2 Axisymmetric model

Under the lubrication approximations with the same assumptions of fully developed, axisymmetric, steady, incompressible laminar flow in a circular deformable tube of radius R (Diameter D) as used by Garg [1] and governing equations, the volume flow rate in a deformable nanotube is given by [1]

$$Q = \int_0^{R(x)} u \; 2\pi \; r \; dr = -\frac{\partial p}{\partial x}\frac{\pi R^4}{8\eta} - \lambda\pi\frac{\partial p}{\partial x}\frac{R^3}{2\eta}, \tag{2}$$

where $\lambda \geq 0$, is the slip length [31]. The η and ρ are the viscosity and density of confined water, respectively. As we know from the linear pressure-diameter relationship, i.e., from equation (1), that

$$A = \left(\frac{p}{\beta} + \sqrt{A_o}\right)^2, \tag{3}$$

where $A = \pi R^2$, and $A_o = \pi R_o^2$. Substituting equation (3) in equation (2), we get

$$Q = -\frac{\partial p}{\partial x}\left[\frac{1}{8\pi\eta}\left(\frac{p}{\beta} + \sqrt{A_o}\right)^4 + \lambda\frac{1}{2\eta\sqrt{\pi}}\left(\frac{p}{\beta} + \sqrt{A_o}\right)^3\right]. \tag{4}$$

We consider $p(x = 0)$ as the relative inlet pressure in relation to the pressure at the tube outlet, where $p(x = L) = 0$. In the case of nanotubes, both viscosity ($\eta(D)$) and density ($\rho(D)$) depend on the tube's diameter [1, 15, 16]. When the tube wall experiences small displacements, we assume that the viscosity and density can be approximated as $\eta(D) \sim \eta(D_o)$ and $\rho(D) \sim \rho(D_o)$,

https://doi.org/10.26434/chemrxiv-2023-k7mws **ORCID:** https://orcid.org/0000-0003-4544-7036 Content not peer-reviewed by ChemRxiv. **License:** CC BY-NC-ND 4.0

respectively. We then perform an integration of equation (4) over the tube's length, resulting in the following

$$\int_x^L Q dx = \int_0^{p(x)} \left[\frac{1}{8\pi\eta} \left(\frac{p}{\beta} + \sqrt{A_o} \right)^4 + \lambda \frac{1}{2\eta\sqrt{\pi}} \left(\frac{p}{\beta} + \sqrt{A_o} \right)^3 \right] dp, \tag{5}$$

$$\implies (L-x)Q = \frac{\beta}{40\pi\eta} \left[\left(\frac{p}{\beta} + \sqrt{A_o} \right)^5 - \sqrt{A_o}^5 \right] + \frac{\lambda\beta}{8\eta\sqrt{\pi}} \left[\left(\frac{p}{\beta} + \sqrt{A_o} \right)^4 - \sqrt{A_o}^4 \right]. \tag{6}$$

As the flow rate Q is not a function of longitudinal directional. Therefore substituting $x = 0$ in equation (6) gives

$$Q = \frac{1}{L} \left(\frac{\beta}{40\pi\eta} \left[\left(\frac{\Delta p}{\beta} + \sqrt{A_o} \right)^5 - \sqrt{A_o}^5 \right] + \frac{\lambda\beta}{8\eta\sqrt{\pi}} \left[\left(\frac{\Delta p}{\beta} + \sqrt{A_o} \right)^4 - \sqrt{A_o}^4 \right] \right), \tag{7}$$

where $p(x = 0) = \Delta p$. Therefore the mass flow rate can be written as

$$\dot{m}_{\text{deformable}} = \rho Q = \frac{\rho(D_o)}{\eta(D_o)\ L} \left(\frac{\beta}{40\pi} \left[\left(\frac{\Delta p}{\beta} + \sqrt{A_o} \right)^5 - \sqrt{A_o}^5 \right] + \frac{\lambda\beta}{8\sqrt{\pi}} \left[\left(\frac{\Delta p}{\beta} + \sqrt{A_o} \right)^4 - \sqrt{A_o}^4 \right] \right), \tag{8}$$

where $\rho(D_o)$, and $\eta(D_o)$ are the density and viscosity of nanoconfined water, which are the function of the diameter of the tube as described in the following section 2.3.

2.3 Microstructure of confined water

We use the same density, viscosity, and slip length models as used by Garg [1] from Garg and Bishnoi [32] where for the density $\frac{\rho(D)}{\rho_o} = a + \frac{b}{(D-c)^n}$,. the $\rho_o = 1000$ kg/m^3, $a = 1$, $b = -7.96$ X 10^{-10} m, $c = -1$ X 10^{-10} m, and $n = 1$. Also, for viscosity, $\frac{\eta(D)}{\eta_o} = a + \frac{b}{(D-c)^n}$, at temperature 298 K as shown by Garg and Bishnoi [32] on the solid-green line, they get $\eta_o = 1$ mPa-s, $a = 0.9$, $b = -3.21$ X 10^{-10} m, $c = 1$ X 10^{-10} m, and $n = 1$. We model for tube diameter $D \geq 25$ Å in this study, for that, the slip length is approximately constant. Although multiple studies reported this constant to be between 50nm to 300nm Garg and Bishnoi [32]. When the tube wall undergoes minor displacements, we make the assumption that the density and viscosity, denoted as $\rho(D)$ and $\eta(D)$, respectively, to be approximately, $\rho(D_o)$ and $\eta(D_o)$. Subsequently, we employ these experimental parameters to characterize the flow rate within deformable nanotubes, as discussed in the following section referred to as Section 3.

3 Results and discussion

Using equations (8), the mass flow rate for the deformable wall N carbon tubes using the microstructure properties of confined water can be written as

https://doi.org/10.26434/chemrxiv-2023-k7mws ORCID: https://orcid.org/0000-0003-4544-7036 Content not peer-reviewed by ChemRxiv. License: CC BY-NC-ND 4.0

$$\dot{m}_{\text{deformable}} = \frac{N\rho(D_o)}{\eta(D_o)\ L}\left(\frac{\beta}{40\pi}\left[\left(\frac{\Delta p}{\beta}+\sqrt{A_o}\right)^5-\sqrt{A_o}^5\right]+\frac{\lambda\beta}{8\sqrt{\pi}}\left[\left(\frac{\Delta p}{\beta}+\sqrt{A_o}\right)^4-\sqrt{A_o}^4\right]\right). \quad (9)$$

$$\dot{m}_{\text{deformable}} = \frac{N\rho(D_o)}{\eta(D_o)\ L}\left(\frac{\Delta p A_o^2}{8\pi}\left[\frac{1}{5}\left(\frac{\Delta p}{\beta\sqrt{A_o}}\right)^4+\left(\frac{\Delta p}{\beta\sqrt{A_o}}\right)^3+2\left(\frac{\Delta p}{\beta\sqrt{A_o}}\right)^2+2\left(\frac{\Delta p}{\beta\sqrt{A_o}}\right)+1\right]\right.$$
$$\left.+\frac{\lambda\Delta p}{2\sqrt{\pi}}A_o^{3/2}\left[\frac{1}{4}\left(\frac{\Delta p}{\beta\sqrt{A_o}}\right)^3+\left(\frac{\Delta p}{\beta\sqrt{A_o}}\right)^2+\frac{3}{2}\left(\frac{\Delta p}{\beta\sqrt{A_o}}\right)+1\right]\right). \quad (10)$$

From equation (10), we can easily identify the following limits:

I. The mass flow rate in the rigid wall N nanotubes with and without slips, i.e. $1/\beta = 0$: Using equation (10), the mass flow rate for the rigid tube with slips can be written as

$$(\dot{m}_{\text{rigid}})_{\text{slip}} = \lim_{1/\beta\to 0}\left[\frac{N\rho(D_o)}{\eta(D_o)\ L}\left(\frac{\Delta p A_o^2}{8\pi}\left[\frac{1}{5}\left(\frac{\Delta p}{\beta\sqrt{A_o}}\right)^4+\left(\frac{\Delta p}{\beta\sqrt{A_o}}\right)^3+2\left(\frac{\Delta p}{\beta\sqrt{A_o}}\right)^2+2\left(\frac{\Delta p}{\beta\sqrt{A_o}}\right)\right.\right.\right.$$
$$\left.\left.\left.+1\right]+\frac{\lambda\Delta p}{2\sqrt{\pi}}A_o^{3/2}\left[\frac{1}{4}\left(\frac{\Delta p}{\beta\sqrt{A_o}}\right)^3+\left(\frac{\Delta p}{\beta\sqrt{A_o}}\right)^2+\frac{3}{2}\left(\frac{\Delta p}{\beta\sqrt{A_o}}\right)+1\right]\right)\right], \quad (11)$$

$$\implies (\dot{m}_{\text{rigid}})_{\text{slip}} = \frac{N\rho(D_o)}{\eta(D_o)\ L}\left(\frac{\Delta p\ A_o^2}{8\pi}+\lambda\Delta p\frac{A_o^{3/2}}{2\sqrt{\pi}}\right) = \pi\ \Delta p\ \frac{N\rho(D_o)}{\eta(D_o)\ L}\left(\frac{R_o^4}{8}+\lambda\frac{R_o^3}{2}\right), \quad (12)$$

and the flow rate without slips is (i.e., using $\lambda = 0$), we get

$$(\dot{m}_{\text{rigid}})_{\text{no-slip}} = \pi\ \Delta p\ \frac{N\rho(D_o)}{\eta(D_o)\ L}\left(\frac{R_o^4}{8}\right), \quad (13)$$

which from equation (12), and (13), we get the flow enhancement E as,

$$E_{\text{rigid}} = \frac{(\dot{m}_{\text{rigid}})_{\text{slip}}}{(\dot{m}_{\text{rigid}})_{\text{no-slip}}} = \left(1+4\frac{\lambda}{R_o}\right) \quad (14)$$

the above expression (14) is well known and also described in Kannam et al. [16], Whitby et al. [33]. Further the flow enhancement due to deformable tubes $E_{\text{deformable}}$ can we written by using equations (10) and (13) as

$$E_{\text{deformable}} = \frac{(\dot{m}_{\text{deformable}})_{\text{slip}}}{(\dot{m}_{\text{rigid}})_{\text{no-slip}}} = \left[\frac{1}{5}\left(\frac{\Delta p}{\beta\sqrt{A_o}}\right)^4+\left(\frac{\Delta p}{\beta\sqrt{A_o}}\right)^3+2\left(\frac{\Delta p}{\beta\sqrt{A_o}}\right)^2+2\left(\frac{\Delta p}{\beta\sqrt{A_o}}\right)+1\right]$$
$$+4\frac{\lambda}{R_o}\left[\frac{1}{4}\left(\frac{\Delta p}{\beta\sqrt{A_o}}\right)^3+\left(\frac{\Delta p}{\beta\sqrt{A_o}}\right)^2+\frac{3}{2}\left(\frac{\Delta p}{\beta\sqrt{A_o}}\right)+1\right]. \quad (15)$$

https://doi.org/10.26434/chemrxiv-2023-k7mws **ORCID:** https://orcid.org/0000-0003-4544-7036 Content not peer-reviewed by ChemRxiv. **License:** CC BY-NC-ND 4.0

To our knowledge, we have not seen the above-derived equation (15) in the literature so far. In equation (15), it's evident that the presence of additional non-linear terms, expressed as $\left(\frac{\Delta p}{\beta\sqrt{A_o}}\right)$, due to flexibility, results in an increase in the mass flow rate and hence the flow enhancement.

II. The mass flow rate in the deformable wall N nanotubes without slip, and without confined water properties, i.e. $\lambda = 0$, $\rho(D) = \rho_o$, $\eta(D) = \eta_o$:

$$(\dot{m}_{\text{deformable}})_{\text{no-slip}} = \frac{N\rho_o}{\eta_o\ L}\left(\frac{\Delta p\ A_o^2}{8\pi}\left[\frac{1}{5}\left(\frac{\Delta p}{\beta\sqrt{A_o}}\right)^4 + \left(\frac{\Delta p}{\beta\sqrt{A_o}}\right)^3 + 2\left(\frac{\Delta p}{\beta\sqrt{A_o}}\right)^2 + 2\left(\frac{\Delta p}{\beta\sqrt{A_o}}\right) + 1\right]\right). \tag{16}$$

Equation (16) is the same as the analytical model derived by Sochi [24] using the second model.

III. The mass flow rate in the rigid wall N nanotubes, without slip and without confined water properties, i.e. $1/\beta = 0$, $\lambda = 0$, $\rho(D) = \rho_o$, $\eta(D) = \eta_o$: Under these limits, we obtain

$$\dot{m}_{\text{rigid}} = \pi\ \Delta p\ \frac{N\rho_o}{\eta_o\ L}\left(\frac{R_o^4}{8}\right), \tag{17}$$

which is a classical result of Hagen-Poiseuille flow in tubes [34–37]. Now, in the following section, we will discuss the effect of deformability and slip on flow enhancement.

3.1 Enhancement and mass flow rate as a function of tube diameter

Using the same literature data as taken by Garg [1], we compare the prediction by our flow rate model using the linear pressure-diameter relationship with pressure $p = 1$ bar, viscosity and density as the fitted confined water properties as described in previous section 2.3, for diameter $D_o \geq 25$ Å , (i.e., Region II, where the slip length does not depend on the diameter and can be assumed constant [16, 32]) as shown in figure 2.

We show the enhancement factor using the dashed red line and dotted green line for rigid wall model at constant $\lambda = 500$ Å , and $\lambda = 3000$ Å , respectively. We further use $\beta = 1 \times 10^{12}$ Pa/m for the deformable tube, and using $\lambda = 500$ Å while keeping other parameters the same as for the rigid wall tube, we calculated the enhancement factor (by using equation (15)) as shown with the solid black line. Similar to Garg [1], we also find that many observations and MD predictions, such as the results by McGinnis et al. [9], Secchi et al. [10], Thomas and McGaughey [38], Borg et al. [39], Kim et al. [40] are well fitted with the rigid wall tube model. On the other hand, the results and MD predictions by Majumder et al. [15], Baek et al. [17], Zhang et al. [18], Majumder et al. [19], Majumder and Corry [20], Trivedi and Reecha [21], Lee et al. [22], Bui et al. [23] are well fitted with the deformable wall tube model. In the later data set, researchers used thin tube structure where deformability of the wall plays an important role to increase flow rate manifold.

Utilizing a linear pressure-diameter relationship for deformability, in contrast to the linear pressure-area relationship used by Garg [1], we also observe a corresponding increase in flow rate as the deformability $1/\beta$, increases. However, it's worth noting that the scaling of flow rate differs from what Garg [1] reported using the linear pressure-area deformability model.

https://doi.org/10.26434/chemrxiv-2023-k7mws **ORCID:** https://orcid.org/0000-0003-4544-7036 Content not peer-reviewed by ChemRxiv. **License:** CC BY-NC-ND 4.0

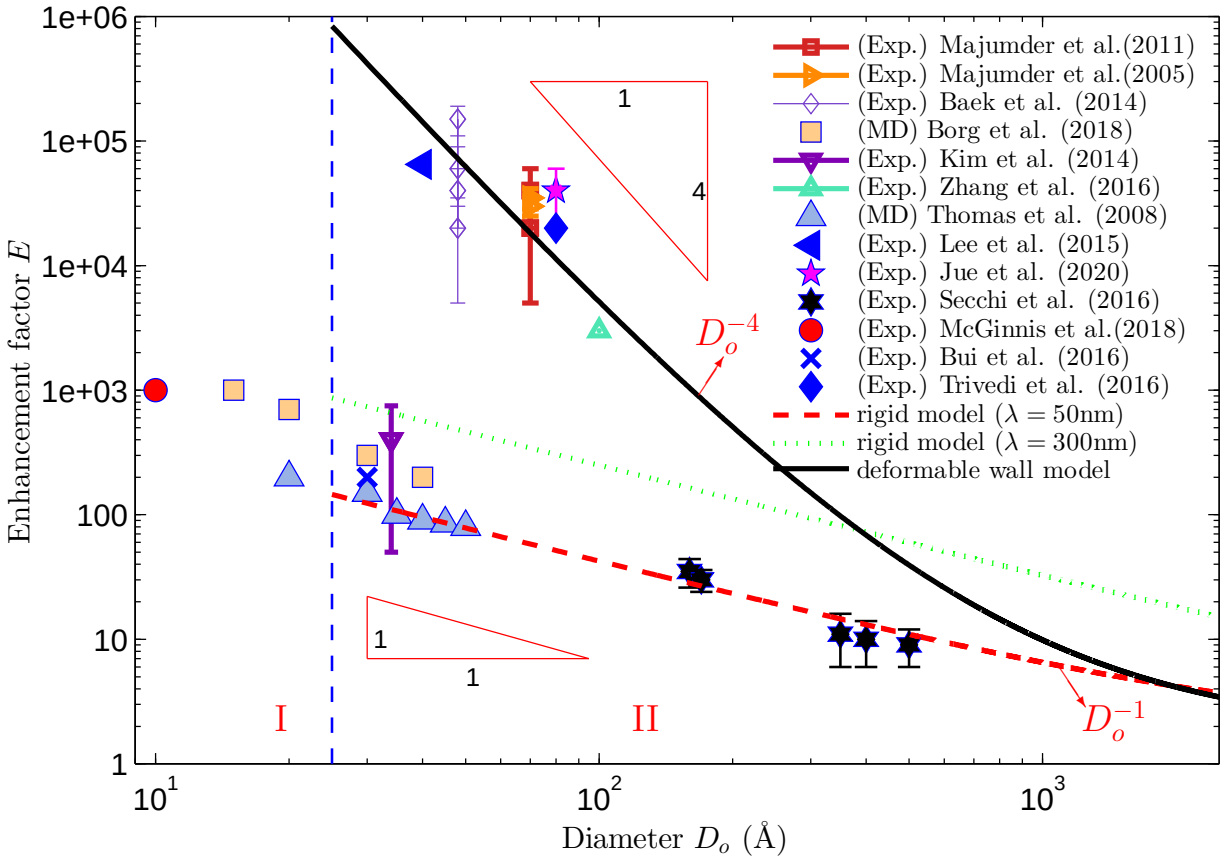

Figure 2: We show the enhancement factor using the rigid tube model (dashed red and dotted green with $\lambda = 500$ Å , and $\lambda = 3000$ Å , respectively), and the deformable tube model (solid black line) as a function of the diameter of the nano/Angstrom-sized tubes and compared with many previous experimental results and Molecular Dynamic simulation's predictions (shown with various symbols) on the log-log scale. Here, for diameter $D_o \geq 25$ Å , i.e., Region II, the slip length does not depend on the diameter and can be assumed constant [16, 32].

Our findings indicate that the flow rate in deformable tubes follows specific scaling behaviors: $\dot{m}_{\text{deformable}} \sim 1/\beta^0$ when $\left(\Delta p/\beta\sqrt{A_o}\right) \ll 1$, $\dot{m}_{\text{deformable}} \sim 1/\beta$ when $\left(\Delta p/\beta\sqrt{A_o}\right) \sim O(10^{-1})$, and $\dot{m}_{\text{deformable}} \sim 1/\beta^4$ when $\left(\Delta p/\beta\sqrt{A_o}\right) \sim O(1)$. Additionally, we find that for a given deformability factor β, the enhancement factor E in smaller diameter tubes is significantly higher than in larger diameter tubes. As the tube diameter decreases under a given reservoir pressure, the enhancement factor E first increases as D_o^{-1} and then as D_o^{-4} after surpassing a certain threshold diameter.

3.2 Effect of deformability on mass flow rate

Using diameter $D_o = 30$ Å , length $L = 1000$ Å , $\lambda = 500$ Å , and same experimental parameters as in previous section, we show the mass flow rate as a function of varying reservoir pressure in figure 3. The β is increasing (corresponding deformability is decreasing) from the green line to the purple line, respectively. We find that for the large deformability parameter $\beta = 10^{23}$, where

https://doi.org/10.26434/chemrxiv-2023-k7mws **ORCID:** https://orcid.org/0000-0003-4544-7036 Content not peer-reviewed by ChemRxiv. **License:** CC BY-NC-ND 4.0

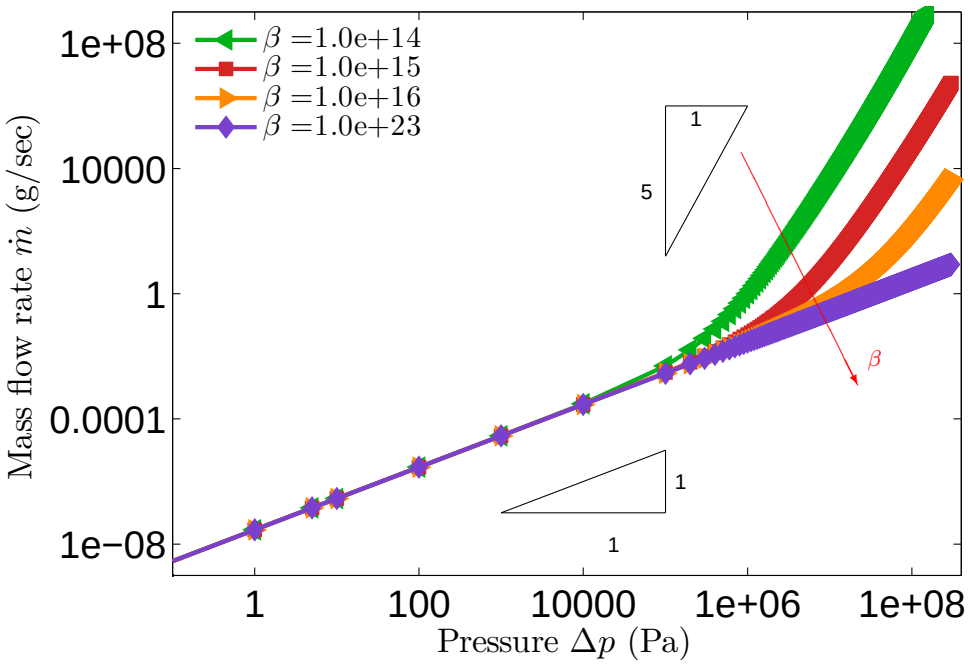

Figure 3: We show the mass flow rate as a function of varying reservoir pressure under varying deformability $(1/\beta)$ of the tube wall on the log-log scale. The red arrow indicates the increasing values of β (corresponding decreasing value of deformability), respectively.

the tube act as rigid, the flow rate varies linearly, i.e., $\dot{m}_{\text{rigid}} \sim \Delta p$ as shown with purple color, whereas for the deformable tubes where the deformability parameter (β) is relatively smaller from orange data to green color data, the flow rate scales as $\dot{m}_{\text{deformable}} \sim \Delta p^2$ for $\left(\Delta p/\beta\sqrt{A_o}\right) \sim O(10^{-1})$ during transition from $\dot{m}_{\text{rigid}} \sim \Delta p$ to $\sim \Delta p^5$, and finally to $\dot{m}_{\text{deformable}} \sim \Delta p^5$ for $\left(\Delta p/\beta\sqrt{A_o}\right) \sim O(1)$ as shown with the black scaling triangles. This suggests that the mass flow rate increases as the deformability of the tube increases. In contrast, with the linear pressure-area relationship for deformable tubes as presented in Garg et al.'s study, the scaling was found to be $\dot{m}_{\text{deformable}} \sim \Delta p^3$ when $\left(\Delta p/\alpha A_o\right) \sim O(1)$ [1].

3.3 Effect of slip on mass flow rate

The mass flow in the deformable tube due to only slip and due to no-slip by using equation (10), can be written as

$$\dot{m}_1 = \frac{N\rho(D_o)}{\eta(D_o)\ L}\left(\frac{\lambda\Delta p}{2\sqrt{\pi}}A_o^{3/2}\left[\frac{1}{4}\left(\frac{\Delta p}{\beta\sqrt{A_o}}\right)^3 + \left(\frac{\Delta p}{\beta\sqrt{A_o}}\right)^2 + \frac{3}{2}\left(\frac{\Delta p}{\beta\sqrt{A_o}}\right) + 1\right]\right), \tag{18}$$

and

$$\dot{m}_2 = \frac{N\rho(D_o)}{\eta(D_o)\ L}\left(\frac{\Delta p\ A_o^2}{8\pi}\left[\frac{1}{5}\left(\frac{\Delta p}{\beta\sqrt{A_o}}\right)^4 + \left(\frac{\Delta p}{\beta\sqrt{A_o}}\right)^3 + 2\left(\frac{\Delta p}{\beta\sqrt{A_o}}\right)^2 + 2\left(\frac{\Delta p}{\beta\sqrt{A_o}}\right) + 1\right]\right), \tag{19}$$

https://doi.org/10.26434/chemrxiv-2023-k7mws ORCID: https://orcid.org/0000-0003-4544-7036 Content not peer-reviewed by ChemRxiv. License: CC BY-NC-ND 4.0

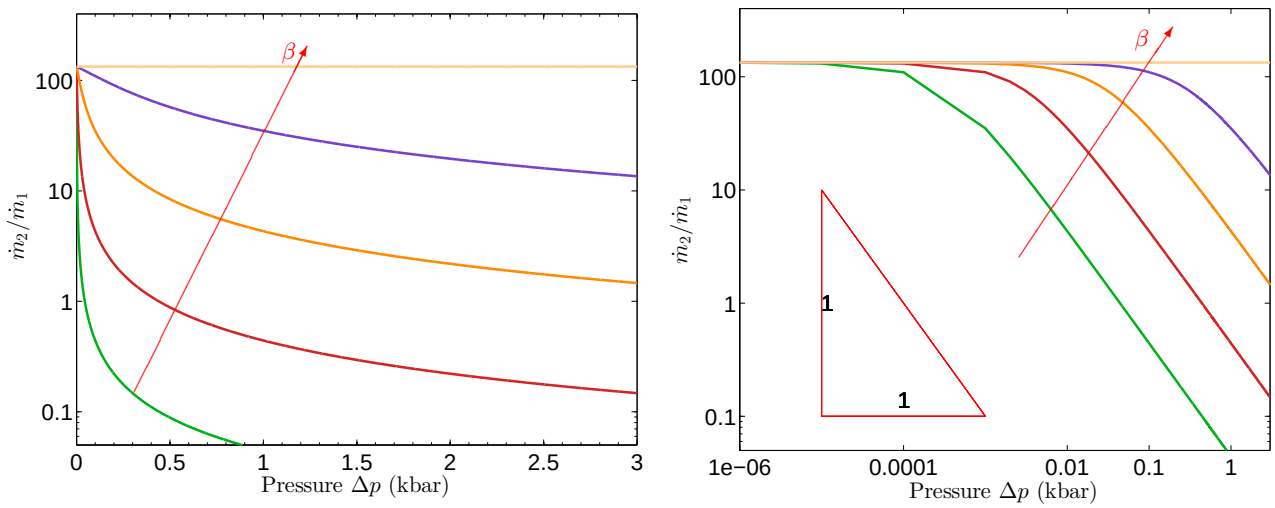

Figure 4: We show the ratio of the mass flow rate in the varying deformability of the tube due to only slip $\dot{m}_1$ and the other due to no-slip $\dot{m}_2$ as a function of varying reservoir pressure. The red arrow indicates the increasing values of β (corresponding decreasing value of deformability), respectively. In (a) and (b), the data is shown on the linear and log-log scale, respectively.

respectively. We keep the other experimental parameters as it is and show the ratio of these mass flow rate on the linear and log-log scale as a function of varying reservoir pressure in figures 4(a), and 4(b), respectively.

Much like the observations made by Garg [1], we also note that at low values of β, such as in the case of the green curve with $\beta = 10^{13}$ Pa/m, where deformability is significantly higher compared to the yellow curve with $\beta = 10^{23}$ Pa/m, the flow rate due to slip is more prominent in comparison to flow without slip. Furthermore, we observe that for low pressure levels, the ratio of these flow rates remains constant regardless of the value of the deformability parameter. As the pressure difference increases, the dependence of this ratio transitions from $\dot{m}_1/\dot{m}_2 \sim \Delta p^0$ to Δp^{-1}. This transition initiates at an early stage of pressure rise, particularly evident in 4(b), where the green data curve is the first to undergo this change, followed by the red curve ($\beta = 10^{14}$ Pa/m), the orange curve ($\beta = 10^{15}$ Pa/m), and ultimately, the yellow curve remains constant under higher pressure conditions. In line with Garg [1]'s findings using a linear pressure-area deformable model, this trend suggests that the impact of mass flow rate due to slip is less significant in more deformable tubes compared to less deformable or rigid tubes.

3.4 Effect of deformability and slip of graphene sheet on the mass flow rate

Using $1/\beta = 0$ m/Pa for rigid tubes and $1/\beta = 10^{-15}$ m/Pa for deformable tubes keeping all experimental parameters as it is, we show the flow rate for the deformable tube ($1/\beta = 10^{-15}$ m/Pa) with slip (i.e., $\lambda = 500$ Å) in green color, with ($1/\beta = 10^{-15}$ m/Pa) without slip (i.e., $\lambda = 0$ Å) in red color, and for the rigid wall tube ($1/\beta = 0$ m/Pa) without slip (i.e., $\lambda = 0$ Å) in purple color in figure 5 as a function of varying pressure, respectively.

In line with the findings of Garg [1], we also observe that the wall's deformability leads to an

https://doi.org/10.26434/chemrxiv-2023-k7mws ORCID: https://orcid.org/0000-0003-4544-7036 Content not peer-reviewed by ChemRxiv. License: CC BY-NC-ND 4.0

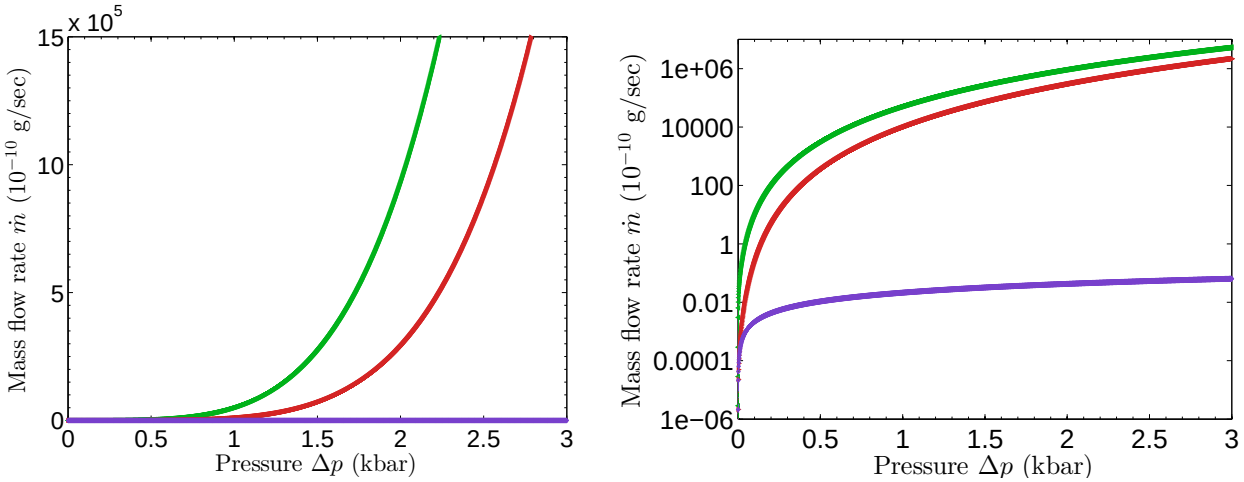

Figure 5: We show the mass flow rate in the rigid and deformable tubes with and without slips as a function of varying reservoir pressure. In (a) and (b), the data is shown on the linear and semilog scale, respectively. The data shown are the mass flow rate for the deformable tube ($1/\beta = 10^{-15}$ m/Pa) with slip (i.e., $\lambda = 500$ Å) in green color, mass flow rate for the deformable tube ($1/\beta = 10^{-15}$ m/Pa) without slip (i.e., $\lambda = 0$ Å) in red color, mass flow rate for the rigid wall tube ($1/\beta = 0$ m/Pa) without slip (i.e., $\lambda = 0$ Å) in purple color, respectively.

increase in the mass flow rate under varying pressure conditions when compared to deformable walls without slip and rigid-walled tubes. For instance, when the pressure difference is $\Delta p = 3$ kbar, the mass flow rate in the deformable tube wall without slips (depicted in red) is 2.16×10^{-4} g/s, while for the rigid tube without slips (represented by purple), it is only 0.06×10^{-10} g/s. This demonstrates that even a slight degree of deformability in the tube significantly enhances the mass flow rate, on the order of approximately 10^7 times, which is a noteworthy increase. Additionally, we find that the difference between the mass flow rate with slips and without slips for deformable tubes is on the order of 10^1 times. This suggests that while slip does increase the flow rate in nanotubes, deformability has a more substantial impact on increasing the mass flow rate.

Furthermore, we observe that as the pressure increases within a deformable tube, the flow rate experiences a substantial increase compared to that in a rigid tube. This phenomenon arises because, in the case of a rigid tube, the mass flow rate exhibits a linear proportionality to Δp. In contrast, in deformable tube, the flow rate (as described in equation (10)) comprises non-linear terms of Δp, causing it to transition from a dependence on Δp to Δp^5 as the pressure increases. Conversely, in the context of a linear pressure-area deformable model, this dependency shifts from Δp to Δp^3 as the pressure rises as predicted by Garg [1].

4 Conclusion

In this paper, we derived a deformable model for nanotubes by using the small displacement structural mechanics through a linear pressure-diameter relationship as presented by the second model in Sochi [24] under the lubrication approximation. For the validation purpose, we show

https://doi.org/10.26434/chemrxiv-2023-k7mws ORCID: https://orcid.org/0000-0003-4544-7036 Content not peer-reviewed by ChemRxiv. License: CC BY-NC-ND 4.0

that the derived model to its limiting cases, which have been given in the literature [16, 24, 33–36]. Similar to Garg [1], we also compare the predictions of our model with the previous experimental results and the MD simulation predictions in literatures and observe that for the studies with high porosity and thin wall tubes, where deformability of the tube is important in modelling were well-predicted by our deformable-wall model with slips [15, 17–23].

Using a linear pressure-diameter relationship for deformability in contrast to linear pressure-area relationship by Garg [1], we also find that as the deformability $1/\beta$ increases, the flow rate also increases. Although the scaling for how the flow rate and flow physics varies are different than reported by Garg [1] with pressure-area model. We find that the flow rate in deformable tubes scales as $\dot{m}_{\text{deformable}} \sim 1/\beta^0$ for $\left(\Delta p/\beta\sqrt{A_o}\right) \ll 1$, $\dot{m}_{\text{deformable}} \sim 1/\beta$ for $\left(\Delta p/\beta\sqrt{A_o}\right) \sim O(10^{-1})$ and $\dot{m}_{\text{deformable}} \sim 1/\beta^4$ for $\left(\Delta p/\beta\sqrt{A_o}\right) \sim O(1)$. We also find that, for a given deformability factor β, the flow rate in the smaller diameter of the tube is much larger than the larger diameter. As the tube diameter decreases for the given reservoir pressure, the flow rate increases D_o^{-1} followed by D_o^{-4} after a threshold with the tube diameter.

We further find that for the rigid tube, where the deformability parameter $1/\beta = 0$, the mass flow rate varies linearly, i.e., $\dot{m}_{\text{rigid}} \sim \Delta p$, whereas for the deformable tubes, the flow rate scales as $\dot{m}_{\text{deformable}} \sim \Delta p^2$ for $\left(\Delta p/\beta\sqrt{A_o}\right) \sim O(10^{-1})$ during transition from $\dot{m}_{\text{rigid}} \sim \Delta p$ to $\sim \Delta p^5$, and finally to $\dot{m}_{\text{deformable}} \sim \Delta p^5$ for $\left(\Delta p/\beta\sqrt{A_o}\right) \sim O(1)$. On the otherhand in case of linear pressure-area relationship for the deformable tubes, the scaling was $\dot{m}_{\text{deformable}} \sim \Delta p^3$ for $\left(\Delta p/\alpha A_o\right) \sim O(1)$ [1].

References

[1] Ashish Garg. Enhanced flow in deformable carbon nanotubes. *ChemRxiv: Nanoscience*, 2023. doi: 10.26434/chemrxiv-2023-j8ndj.

[2] GQ Max Lu and Xiu Song Zhao. *Nanoporous materials: science and engineering*, volume 4. World Scientific, 2004.

[3] Alyson Sagle and Benny Freeman. Fundamentals of membranes for water treatment. *The future of desalination in Texas*, 2(363):137, 2004.

[4] Elton Oyarzua, Jens H Walther, Andrés Mejía, and Harvey A Zambrano. Early regimes of water capillary flow in slit silica nanochannels. *Physical Chemistry Chemical Physics*, 17(22):14731–14739, 2015.

[5] Zohreh Jalilvand, Farzin Zokaee Ashtiani, Amir Fouladitajar, and Hamid Rezaei. Computational fluid dynamics modeling and experimental study of continuous and pulsatile flow in flat sheet microfiltration membranes. *Journal of Membrane Science*, 450:207–214, 2014.

[6] Fatemeh Ebrahimi, Farzaneh Ramazani, and Muhammad Sahimi. Nanojunction effects on water flow in carbon nanotubes. *Scientific Reports*, 8(1):7752, 2018.

[7] Pranay Ashok Asai. *Assessing Fluid Flow in Nanoporous Media and Doublet Multi-Fractured Enhanced Geothermal Systems*. PhD thesis, The University of Utah, 2021.

[8] Jürgen Köfinger, Gerhard Hummer, and Christoph Dellago. Macroscopically ordered water in nanopores. *Proceedings of the National Academy of Sciences*, 105(36):13218–13222, 2008.

[9] Robert L McGinnis, Kevin Reimund, Jian Ren, Lingling Xia, Maqsud R Chowdhury, Xuanhao Sun, Maritza Abril, Joshua D Moon, Melanie M Merrick, Jaesung Park, et al. Large-scale polymeric carbon nanotube membranes with sub–1.27-nm pores. *Science advances*, 4(3):e1700938, 2018.

https://doi.org/10.26434/chemrxiv-2023-k7mws **ORCID:** https://orcid.org/0000-0003-4544-7036 Content not peer-reviewed by ChemRxiv. **License:** CC BY-NC-ND 4.0

[10] Eleonora Secchi, Sophie Marbach, Antoine Niguès, Derek Stein, Alessandro Siria, and Lydéric Bocquet. Massive radius-dependent flow slippage in carbon nanotubes. *Nature*, 537(7619):210–213, 2016.

[11] Pranay Chakraborty, Tengfei Ma, Lei Cao, and Yan Wang. Significantly enhanced convective heat transfer through surface modification in nanochannels. *International Journal of Heat and Mass Transfer*, 136:702–708, 2019.

[12] Jie Sun, Yaling He, Wenquan Tao, Xin Yin, and Huasheng Wang. Roughness effect on flow and thermal boundaries in microchannel/nanochannel flow using molecular dynamics-continuum hybrid simulation. *International journal for numerical methods in engineering*, 89(1):2–19, 2012.

[13] Tristan da Câmara Santa Clara Gomes, Flavio Abreu Araujo, and Luc Piraux. Making flexible spin caloritronic devices with interconnected nanowire networks. *Science advances*, 5(3):eaav2782, 2019.

[14] Vidit Sharma and Ashish Garg. Numerical investigation of effects of compound angle and length to diameter ratio on adiabatic film cooling effectiveness. *arXiv preprint arXiv:1405.0560*, 2014.

[15] Mainak Majumder, Nitin Chopra, Rodney Andrews, and Bruce J Hinds. Enhanced flow in carbon nanotubes. *Nature*, 438(7064):44–44, 2005.

[16] Sridhar Kumar Kannam, BD Todd, Jesper Schmidt Hansen, and Peter J Daivis. How fast does water flow in carbon nanotubes? *The Journal of chemical physics*, 138(9), 2013.

[17] Youngbin Baek, Cholin Kim, Dong Kyun Seo, Taewoo Kim, Jeong Seok Lee, Yong Hyup Kim, Kyung Hyun Ahn, Sang Seek Bae, Sang Cheol Lee, Jaelim Lim, et al. High performance and antifouling vertically aligned carbon nanotube membrane for water purification. *Journal of membrane Science*, 460:171–177, 2014.

[18] Xiuyin Zhang, Chuanzhuang Zhao, Nanping Xiang, and Wei Li. Chain entanglements and hydrogen bonds in carbopol microgel reinforced hydrogel. *Macromolecular Chemistry and Physics*, 217(19):2139–2144, 2016.

[19] Mainak Majumder, Nitin Chopra, and Bruce J Hinds. Mass transport through carbon nanotube membranes in three different regimes: ionic diffusion and gas and liquid flow. *ACS nano*, 5(5):3867–3877, 2011.

[20] Mainak Majumder and Ben Corry. Anomalous decline of water transport in covalently modified carbon nanotube membranes. *Chemical Communications*, 47(27):7683–7685, 2011.

[21] Monika Trivedi and K Reecha. Recent development and applications of carbon nanotubes. *Chem. Sci. Rev. Lett*, 9: 502–510, 2020.

[22] Byeongho Lee, Youngbin Baek, Minwoo Lee, Dae Hong Jeong, Hong H Lee, Jeyong Yoon, and Yong Hyup Kim. A carbon nanotube wall membrane for water treatment. *Nature communications*, 6(1):7109, 2015.

[23] Ngoc Bui, Eric R Meshot, Sangil Kim, José Peña, Phillip W Gibson, Kuang Jen Wu, and Francesco Fornasiero. Ultrabreathable and protective membranes with sub-5 nm carbon nanotube pores. *Advanced Materials*, 28(28):5871–5877, 2016.

[24] Taha Sochi. The flow of newtonian and power law fluids in elastic tubes. *International Journal of Non-Linear Mechanics*, 67:245–250, 2014.

[25] Xiluan Wang and Gaoquan Shi. Flexible graphene devices related to energy conversion and storage. *Energy & Environmental Science*, 8(3):790–823, 2015.

[26] Ashish Garg. Pulsatile pressure enhanced rapid water transport through flexible graphene nano/angstrom-size channels: a continuum modeling approach using the micro-structure of nanoconfined water. *New Journal of Physics*, 25 (10):103024, 2023. doi: 10.1088/1367-2630/acff7e.

[27] Ashish Garg, Nico Bergemann, Beccy Smith, Matthias Heil, and Anne Juel. Fluidisation of yield stress fluids under vibration. *Science Talks*, 3:100067, 2022.

[28] Ashish Garg and Pranjal Prasad. Yield-stress shear thinning and shear thickening fluid flows in deformable channels. *ChemRxiv-Polymer Science, DOI: 10.26434/chemrxiv-2023-jb7xw*, pages 1–19, 2023.

https://doi.org/10.26434/chemrxiv-2023-k7mws **ORCID:** https://orcid.org/0000-0003-4544-7036 Content not peer-reviewed by ChemRxiv. **License:** CC BY-NC-ND 4.0

[29] Ashish Garg and Pranjal Prasad. Wall-slip effects on the yield-stress fluid flows in the rigid and deformable channel. *ChemRxiv-Polymer Science, DOI: 10.26434/chemrxiv-2023-l3knn*, pages 1–30, 2023.

[30] Ashish Garg. Fluidisation of yield stress materials under vibration. *PhD thesis, The University of Manchester*, pages 1–175, 2022.

[31] Barry James Cox and James Murray Hill. Flow through a circular tube with a permeable navier slip boundary. *Nanoscale research letters*, 6:1–9, 2011.

[32] Ashish Garg and Swati Bishnoi. An empirical experimental observations and md simulation data-based model for the material properties of confined fluids in nano/angstrom size tubes. 2023. doi: 10.26434/chemrxiv-2023-s66r8.

[33] Max Whitby, Laurent Cagnon, Maya Thanou, and Nick Quirke. Enhanced fluid flow through nanoscale carbon pipes. *Nano letters*, 8(9):2632–2637, 2008.

[34] Frank M White. *Fluid mechanics*. New York, 1990.

[35] George Keith Batchelor. *An introduction to fluid dynamics*. Cambridge university press, 1967.

[36] Brian J Kirby. *Micro-and nanoscale fluid mechanics: transport in microfluidic devices*. Cambridge university press, 2010.

[37] Ashish Garg. Aerodynamics. In *GATE Aerospace Forum Educational Services*, 2015.

[38] John A Thomas and Alan JH McGaughey. Reassessing fast water transport through carbon nanotubes. *Nano letters*, 8(9):2788–2793, 2008.

[39] Matthew K Borg, Duncan A Lockerby, Konstantinos Ritos, and Jason M Reese. Multiscale simulation of water flow through laboratory-scale nanotube membranes. *Journal of Membrane Science*, 567:115–126, 2018.

[40] Sangil Kim, Francesco Fornasiero, Hyung Gyu Park, Jung Bin In, Eric Meshot, Gabriel Giraldo, Michael Stadermann, Micha Fireman, Jerry Shan, Costas P Grigoropoulos, et al. Fabrication of flexible, aligned carbon nanotube/polymer composite membranes by in-situ polymerization. *Journal of membrane science*, 460:91–98, 2014.

https://doi.org/10.26434/chemrxiv-2023-k7mws **ORCID:** https://orcid.org/0000-0003-4544-7036 Content not peer-reviewed by ChemRxiv. **License:** CC BY-NC-ND 4.0